UDC 681.3 : 536.24.08

*Siberian Journal of Science and Technology.* 2017, Vol. 18, No. 3, P. 592–603

# THE STUDY OF THE FLOW IN THE VAPOUR CHANNEL OF SHORT LINEAR HEAT PIPES

A. V. Seryakov

LLC Research and Development Company "Rudetransservice",
55, Nekhinskaya Str., Veliky Novgorod, 173025, Russian Federation
E-mail: seryakovav@yandex.ru

*The results of studies of flow of moist vapour in Laval-like vapour channels of short linear heat pipes (HPs) are presented. The increase in heat transfer coefficient of short linear HPs, intended for creation of the cooling systems of heat-stressed designs of spacecraft, is carried out by making the HPs vapour channel forms similar to the shape of the Laval-like nozzle. Comparison of the heat transfer coefficients of short HPs with the standard cylindrical vapour channel and the channel, made in the form of the Laval-like nozzle with the equality of all dimensions, flat evaporator and the same amount of the working fluid, shows that the HPs with the vapour channel in the form of the Laval-like nozzle exceeds the heat transfer characteristics of the standard HPs with a cylindrical vapour channel under high thermal loads. The study of the flow and condensation in such shaped vapour channels of the short HPs at high thermal loads gives an opportunity to analyze in detail the advantages of using such HPs and make the conclusion about the necessity of wide introduction of such HPs for the cooling systems of the spacecraft. Capacitive sensors were additionally installed in cooled top covers of the HPs, and electromagnetic pulses with a frequency of 100 kHz were supplied to them from the external generator. At heating the HPs evaporator, starting from a certain thermal power threshold value, electromagnetic pulses became modulated. It is related to the formations of the boiling process in the capillary-porous evaporator and large amount of vapour over it and its discontinuous distribution. It was discovered that the frequencies of the pulsations are more and they occur at lower values of heat load at the evaporator in the HPs with a vapour channel of a Laval-like nozzle, compared to the HPs with the standard cylindrical vapour channel with equal overall dimensions.*

*Keywords: Heat pipes, Laval nozzle, pulsation, heat transfer coefficient.*

Сибирский журнал науки и технологий. 2017. Т. 18, № 3. С. 592–603

# ИССЛЕДОВАНИЕ ТЕЧЕНИЙ В ПАРОВОМ КАНАЛЕ КОРОТКИХ ЛИНЕЙНЫХ ТЕПЛОВЫХ ТРУБ

А. В. Серяков

ООО «Рудетранссервис»
Российская Федерация, 173025, г. Великий Новгород, ул. Нехинская, 55
E-mail: seryakovav@yandex.ru

*Представлены результаты исследований течения влажного пара в выполненных в виде сопла, близкого к соплу Лаваля, паровых каналах коротких линейных тепловых труб (ТТ).*

*Повышение коэффициента теплопередачи коротких линейных ТТ, предназначенных для создания систем охлаждения теплонапряженных конструкций космических аппаратов, осуществляют за счет придания паровому каналу ТТ формы сопла, близкого к соплу Лаваля.*

*Сопоставление коэффициентов теплопередачи коротких ТТ со стандартным цилиндрическим паровым каналом и с выполненным в виде сопла, близкого к соплу Лаваля, паровым каналом при равенстве всех габаритных размеров, плоском испарителе и одинаковом количестве рабочей жидкости показывает, что ТТ с паровым каналом в виде сопла, близкого к соплу Лаваля, превосходят в теплопередающих характеристиках стандартные ТТ с цилиндрическим паровым каналом при высоких тепловых нагрузках. Изучение особенностей течений и конденсации в таких профилированных паровых каналах коротких ТТ при высоких тепловых нагрузках дает возможность детально проанализировать преимущества применения подобных ТТ и сделать вывод о необходимости их широкого внедрения для систем охлаждения космических аппаратов.*

*В охлаждаемые верхние крышки ТТ дополнительно установлены емкостные датчики, на электроды которых от внешнего генератора были поданы электромагнитные импульсы частотой 100 кГц. При нагревании испарителей ТТ, начиная с некоторой пороговой тепловой нагрузки, электромагнитные импульсы становятся модулированными. Это связано с началом кипения в капиллярно-пористом испарителе, образованием большого количества пара и его прерывистым распространением. Обнаружено, что частоты пульсаций больше и возникают они при меньших величинах тепловой нагрузки на испаритель в ТТ с паровым каналом, выполненном*

*в виде сопла, близкого к соплу Лаваля, по сравнению с ТТ со стандартным цилиндрическим паровым каналом при равных габаритных размерах.*

*Ключевые слова: тепловые трубы, сопло Лаваля, пульсации, коэффициент теплопередачи.*

**Introduction.** The increase of heat transfer coefficient of short linear HPs is a very important task when designing a spacecraft with a rigid regulation of take-off weight. The application of the linear HPs is justified in case of structural impossibility of placing a loop (contoured) HPs for it can improve long-term reliability of the cooling systems, which are distributed inlet and outlet closed lines of the loop (contour) HPs.

Pulsating (or oscillating) loop HPs – siphons, was invented in 1990 by Akachi [1]. When the temperature difference between evaporator and condenser exceeds a certain threshold, Tong et al. [2], R. Naik, et al. [3], the vapour bubbles and condensate liquid plugs begin to oscillate spontaneously back and forth. The amplitude of oscillations is quite strong and the liquid plugs penetrate into both condenser and evaporator. The heat is thus transferred not only by the latent heat transfer liquid-vapour-liquid like in other types of heat pipes, but also by conductive heat transfer of the hot oscillating liquid plugs to cold walls in the condensation zone of loop HPs. This phenomenon is the reason of high heat transfer coefficient of loop HPs in comparison with other types of HPs.

The increase of the heat transfer coefficient in short linear open HPs with capillary porous insert is achieved using inner vapour channel of Laval-liked nozzle form. There is an availability to use a jet vapour nozzle, similar to the Laval nozzle, surrounded by a capillary-porous insert along the full length of the HPs, in case if the heat flow is axially directed that is typical for short HPs. The shape of this vapour Laval-like channel, is defined by the inner capillary porous insert. The implementation of the nozzle increases flow velocity [4], pulse rate of two-phase vapour flow and heat-transfer coefficient in the HPs. Pulsation of the flow in short linear HPs with the capillary porous insert represents more complex phenomena, associated with boiling of the working fluid in the capillary porous evaporator.

Heat-transfer coefficient and operational effectiveness of short linear HPs with capillary-porous inserts and Laval-like vapour channel are defined by closed circulation motion of the working fluid, which undergoes liquid-vapour transition and heat absorption in the evaporation region of the capillary porous insert, vapour phase transfer through a convergent-divergent vapour channel, vapour-liquid transition with heat liberation in the condensation region, and liquid return to the evaporation region through capillary-porous inserts of the HP.

Improvement of the heat-transfer coefficient of heat pipes is a complex task, concerning the device's detailed mechanical design and gas dynamics. Flowing vapour, with microdrops of condensate, appears as a nonlinear flow, with attendant internal processes, such as interphasic heat and mass exchange, and power dissipation, Gupta et all [5]. Static regain of supersaturated vapour flow in the diffuser condensation region of the HPs with turbulator, causes flow stagnation, strong vorticity production near the condensation surface and reverse vapour flow. Thermal load-related processes of vorticity formation and density and pressure fluctuation, proceeding in the convergent-divergent vapour channel of HPs, are of the utmost interest. For a field research of these processes, stainless steel heat pipes have been manufactured with diethyl ether as the working fluid [6–9].

**Materials and methods.** The diethyl ether $C_4H_{10}O$ is selected as the main working fluid, which has the boiling temperature $T_B$ = 308.55 K (35.4 °C) under the atmospheric pressure, freezing temperature $T_F$ = 156.95 K (−116.2 °C) and critical parameters $T_C$ = 466.55 K (193.4 °C), $P_C$ = 3.61 MPa. Successful use of diethyl ether as the working fluid for Wilson chambers, on long liquid phase at 413.15 K (140 °C), shows its heat resistance and allows using it as the HP working fluid.

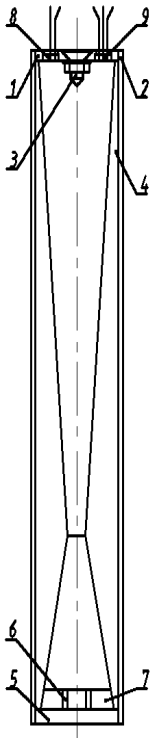


Fig. 1. Layout of HP equipped with capacitance sensors:
*1* – flat upper lid with a smooth surface; *2* – cylinder body of HP; *3* – cone-shaped turbulence agitator; *4* – capillary-porous insert defining the vapour channel's form; *5* – flat bottom lid; *6* – injector channels; *7* – capillary-porous evaporator; *8*, *9* – capacitance sensors, one of which is intended for a condensate film thickness measurement, while another one has a sensing element of CT3-19 thermistor mounted on its electrodes to measure the film temperature [11]

Рис. 1. Схема тепловых труб:
*1* – верхняя крышка; *2* – цилиндрический корпус ТТ; *3* – конический турбулизатор; *4* – капиллярно-пористая вставка; *5* – нижняя крышка; *6* – инжекторные каналы; *7* – капиллярно-пористый испаритель; *8*, *9* – емкостные датчики конденсации, измеряющие толщину слоя жидкого конденсата. Измерительная поверхность емкостных датчиков совпадает с внутренней поверхностью плоской верхней крышки

The developed sensor enables us to perform measurements of local characteristics of the film flows primarily, the film thickness and temperature, without making any major disturbances in the flow. To measure the fluid condensate of film thickness, short HPs were used with vapour channel made in the form of a Laval-like nozzle [10–12]. The HPs are described in details below.

The capillary-porous evaporator *7* is constructed of 43 circular layers of thin stainless steel net (fig. 1). Each layer is 0.07 mm thick with the mesh size of 0.04 mm and the aggregate thickness of 3 mm; all layers are spot-welded to the flat bottom lid *5*. Outer diameters of the circular layers gradually decrease in such a manner that the lateral side of the assembled evaporator forms a pointed cone with a 45° total point angle that aligns with the angle of the end part of the capillary-porous insert *4*. The evaporator as a whole is further equipped with *4* vapour injection channels *6* with increasing diameter of 1 mm, 1.1 mm, 1.2 mm and 1.3 mm diameter that are inclined to the longitudinal axis of HP at a specific angle and create a swirling jet stream of vapour.

The capillary-porous insert *4* is assembled on a dedicated profiled frame made of layers of thin stainless steel net same as the evaporator. Each layer is 0.07 mm thick with mesh size of 0.04 mm, the total thickness of the insert is 1.5 mm at the edges and 7.5 mm at the critical diameter of the inner nozzle. All layers of the insert are radially stitched together along the forming insert with a thin wire 0.05 mm in diameter and stitch spacing of 5–7 mm. Eight lines of the wire stitches that radially fix the net layers together are tilted by 45° towards each other and form a rigid structure of the capillary-porous insert with an inner vapour channel made in the form of a nozzle, similar to the Laval nozzle. At the edge of insert *4* that is adjacent to the evaporator *7*, an end portion is placed; its total angle is somewhat wider than that of the diffuser portion of the vapour channel and equals 45°. The longitudinal length of the end portion is 3 mm and matches the thickness of the evaporator *7* exactly. The 45° angle of the end portion of insert *4* is formed by the gradually decreasing net layers' lengths, from the outer layer to the inner one, and matches the angle of the evaporator *7* exactly. The multilayered evaporator with a tapering lateral side is tightly inserted into the rigid capillary-porous insert *4* at the full length of the end portion and is spot-welded to it in *8* spots along the perimeter of the insert. After being cooled down at the boiling temperature of fluid nitrogen 77 K (–196 °C), the assembled capillary-porous insert together with the evaporator on the flat bottom lid 5 is tightly inserted in the stainless steel cylindrical shell *2* of the HP.

Porosity of the insert and evaporator is 72 % and together they form one hydraulic system designed to deliver the service fluid to the evaporator when the HP is operating. The HP length is 100 mm, its diameter is 20 mm, the max. diameter of the vapour nozzle in the convergent and divergent regions is 16 mm, the critical nozzle diameter is 4 mm, the length of the nozzle convergent region is 13 mm, the total angle of the convergent region is 41°, the length of the nozzle divergent region is 81 mm, the total angle of the divergent region is 8.5°, and the length of the cylindrical region in the nozzle throat section is 1 mm.

**Measurement of the heat transfer coefficient.** Condensation zones of the HPs are provided with insulated thermocouples and set into the vortex continuous-flow calorimeter, shown in fig. 2, with stabilized water flow. To ensure accurate measuring of thermal power and heat removal augmentation in the HPs, jet flow of input water is swirled, values of flow velocity and vorticity due to air bubbles are recorded. The HPs evaporators, also equipped with thermocouples, is heated using a resistance heater, and the temperature is maintained at $\delta T$ °C higher than the diethyl ether boiling temperature of 308.55 K (35.4 °C) under atmospheric pressure. The heater temperature is stabilized and HPs evaporator's overheat value is set in the range of $\delta T$ = 0–20 K, herewith thermal power of single HP does not exceed 120 W.

Measurement were performed to disclose variability of the heat transfer coefficients in Laval-like HPs and with standard cylindrical vapor channel. The heat transfer coefficients in HPs, Faghri [13] is defined by the formula:

$$K_{\text{HP}} = \frac{E}{F(z)\left(T_{ev} - T_{cond}\right)}, \qquad (1)$$

where $K_{\text{HP}}$ is heat transfer coefficient of the HPs, W/K; $E$ is thermal power, supplied in the evaporator of the HPs, W; $F(z)$ is surface area of the evaporator inside the vapour channel of the HPs, m$^2$; $T_{ev}$ is temperature of the evaporator, K; $T_{cond}$ is temperature of the condensation surface, K.

Temperature of evaporator surface and condensation surface of HPs were measured using differential thermocouples copper-constantan, heat power $E$, W; transferred by condensations zones of HPs to the calorimeter, was defined by the formula:

$$E = G \cdot \left( C_{\text{H}_2\text{O}} - \frac{C_K}{\rho_{\text{H}_2\text{O}} V_0} \right) \cdot \left[ T_K(\tau) - T_{K0}(\tau) \right], \qquad (2)$$

where $G$ is water flow in a vortex flow calorimeter, kg/s; $C_{\text{H}_2\text{O}}$ is the specific heat of water, J/kg·K; $C_K$ – the heat capacity of the calorimeter, J/K; $\rho_{\text{H}_2\text{O}}$ is the density of water in the calorimeter, kg /m$^3$; $V_0$ is the internal volume of the calorimeter, m$^3$; $T_{K0}(\tau)$, $T_K(\tau)$ is the water temperature at the inlet and outlet of the calorimeter, K.

Input temperature of water at the calorimeter, temperature differences (heat value) of the flowing water at entrance and exit of the calorimeter were also measured using differential thermocouples copper-constantan, comparator P3003 and digital voltmeter V7-34A. Water flow rate was measured using ultrasonic flowmeter. Total measuring inaccuracy of the thermal power $E$ of the HPs does not exceed 1.7 %.

Comparison of heat transfer coefficients in Laval-like HPs and HPs with standard cylindrical vapour channel with the equality of all dimensions showed following results, presented in fig. 3.

The increase of the heat transfer coefficient in the HP with a Laval-like vapour channel appears to be related to the emergence of a vortex ring near the condensation surface of the HP.

**Numerical model details.** Numerical simulations of the vortex flows inside a vapour channel of the Laval-like HPs have been performed in finite element modeling in CFD 10.0 code Fluent 6.3.26 2D under double precision axis-symmetric conditions. Navier–Stokes equations with measured boundary conditions were solved, i. e. using fixed temperature values of heat source and heat outlet. In the construction of the design model we used about 457233 finite elements with increased meshing at injection capillary channels sections, nozzle throat section and turbulence element. Fig. 4 shows a diagram of the vortex obtained by numerical simulation of CFD 10.0 code.

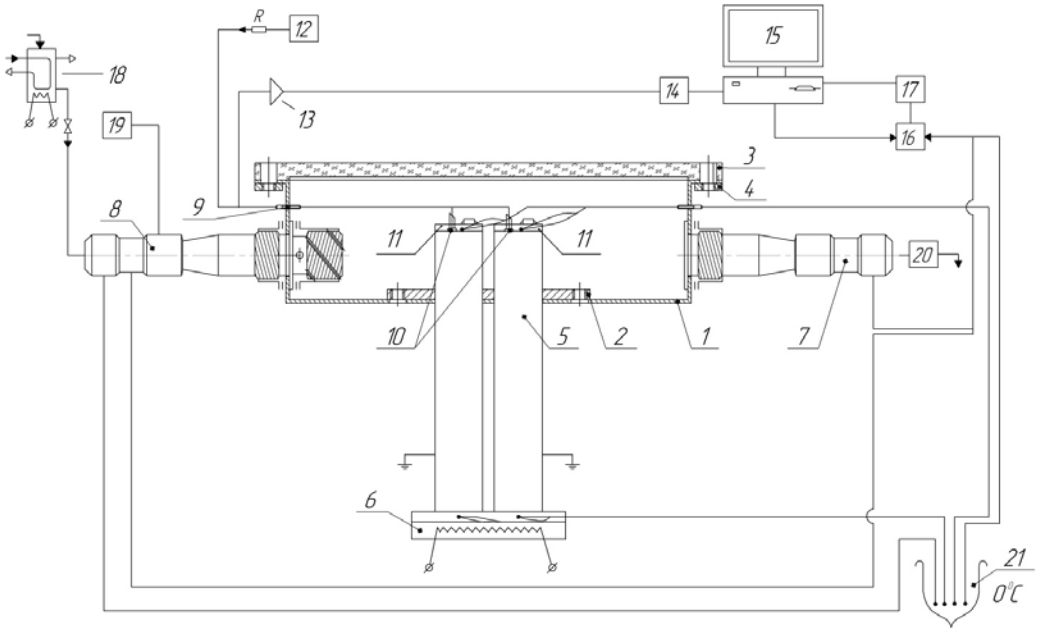


Fig. 2. Vortical calorimeter: *1* – vortical continuous-flow calorimeter; *2* – heat pipes bolting flange; *3* – glass cover; *4* – cover fastening; *5* – heat pipes; *6* – resistance heater; *7* – outlet stub tube for water flow; *8* – inlet stub tube for water flow; *9* – silicone sealant of the sensing wire; *10* – capacitive sensors for measuring the thickness of the condensed layer of the working fluid; *11* – the measuring and reference generators of the capacitive transducer; *12* – external digital generator; *13* – power assist element; *14* – digital oscilloscope; *15* – computer; *16* – commutation switch; *17* – digital voltmeter; *18* – container for constant water head; *19* – source of air bubble; *20* – water flow meter; *21* – vacuum-jacketed zero temperature container

Рис. 2. Вихревой калориметр: *1* – вихревой проточный калориметр; *2* – фланец крепления тепловых труб; *3* – стеклянная крышка; *4* – крепление крышки; *5* – тепловые трубы; *6* – резистивный нагреватель; *7* – выходной штуцер для воды; *8* – входной штуцер для воды; *9* – уплотнение измерительных проводов; *10* – конденсаторные датчики измерения толщины слоя конденсата; *11* – высокочастотные генераторы; *12* – генератор импульсов Г5-56; *13* – усилитель; *14* – осциллограф АКИП-4116/2; *15* – компьютер; *16* – коммутатор; *17* – вольтметр В7-34А; *18* – сосуд постоянного напора воды; *19* – генератор пузырьков воздуха; *20* – расходомер воды; *21* – сосуд Дьюара

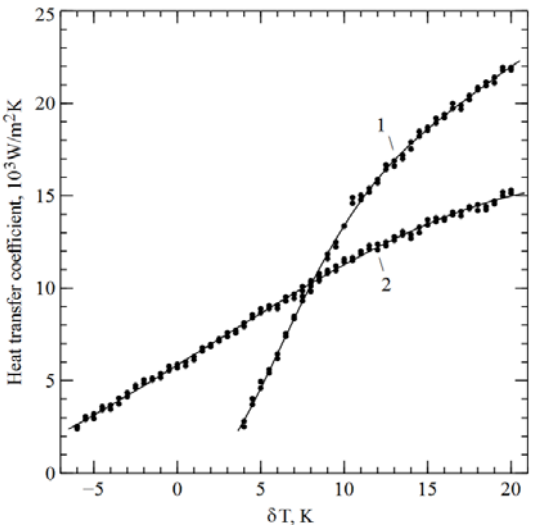


Fig. 3. Comparison of heat transfer coefficients in Laval-like HP and HP with standard cylindrical vapour channel: *1* – Laval-like HPs; *2* – HPs with standard cylindrical vapour channel

Рис. 3. Сравнение коэффициентов теплопередачи ТТ с паровым каналом в виде сопла, близкого к соплу Лаваля, и ТТ с цилиндрическим паровым каналом при равных габаритных размерах: *1* – ТТ с паровым каналом в виде сопла; *2* – ТТ со стандартным паровым каналом

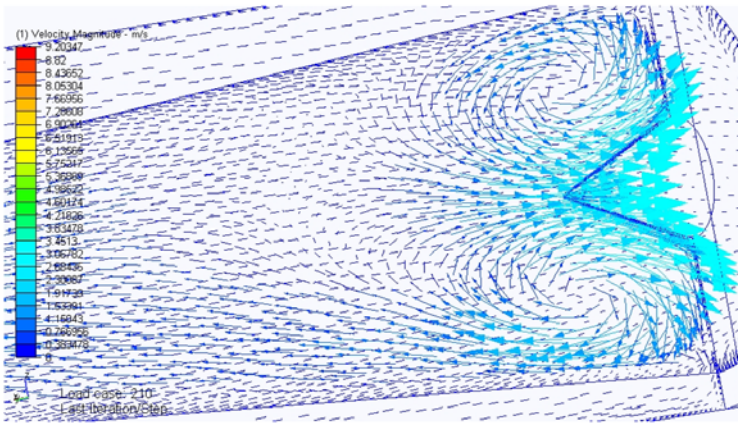


Fig. 4. The occurrence of a vortex ring near the condensation surface inside of Laval-like HPs. The numerical analysis of the flow in the Laval-like HPs condensation zone shows that the vortex structure has a spatial nature, at the same time the flow asymmetry becomes apparent being determined by non-linear friction against the underlying surface and the two-dimensional compressibility of the wet condensing vapour as well. Overheating of the evaporator in reference to the boiling temperature of diethyl ether at atmospheric pressure is 15 K, the temperature difference between the evaporator and the condensation surface equals 25 K

Рис. 4. Возникновение вихревого кольцевого течения вблизи поверхности конденсации вокруг турбулизирующего элемента внутри ТТ с паровым каналом в виде сопла, близкого к соплу Лаваля. Перегрев испарителя относительно температуры кипения диэтилового эфира 15 К, разница температур между испарителем и поверхностью конденсации ТТ в калориметре 25 К

Fig. 5 shows the results of numerical analysis of the distribution of the longitudinal component of the velocity of compressible moist vapour within the Laval-like HP. The formation of a wet condensing vapour vortex ring near the condensation surface inside of Laval-like HPs leads to quite interesting results. Vortex ring is a highly gradient zone of the condensable moist vapour velocity with the opposite directions inside and outside the vortex ring. The numerical analysis of the velocity distribution along the centerline of the vapour channel in the Laval-like HPs including the vortex ring shows the occurrence of two positive peaks of the velocity, one of them is in the critical section of the nozzle and the other is near the condensation surface. In a critical section of the nozzle the axial component of velocity reaches 85 m/s, and near the condensation surface the counter-flow reaches the velocity of 33 m/s. The distribution of the axial component of velocity of the moist vapour shows the presence of a counter current due to the formation of a ring vortex within the vapour channel near the HPs condensation surface. This figure of the velocity distribution, shown in fig. 5, confirms the fact that the vortex ring is a zone of sharp velocity gradients, and consequently is a pressure gradient. In the central part the vortex ring has a noticeable positive dynamic pressure, and it has a negative dynamic pressure in the peripheral part of the vortex ring. This means that lower static pressure occurs in the central part of the vortex ring and this leads to additional absorption of moist vapor in the condensation zone of Laval-like HPs.

Apparently, this means that the static pressure in the vortex center in the Laval-like HP is less than the pressure in the axial part of the condensation zone of the HP with standard cylindrical vapor channel. The appearance of high static pressure in the peripheral part of the vortex ring, where there is a negative dynamic pressure leads to intensification of the condensation process near the top cap of the Laval-like HPs that leads, apparently, to an increased value of heat transfer coefficient in the Laval-like HPs. This explains the reason why the heat transfer coefficient of Laval-like HPs becomes greater than that of HPs with the cylindrical vapor channel at boiling point in evaporator HP and there is formation of large amounts of vapor and increase in the efficiency of the nozzle in comparison with a cylindrical channel.

**Measurement of pulse characteristics of HPs.** The pulsation characteristics of HPs were measured and discussed previously [6; 7]. Starting from the specific overheating $\delta T_S = (T - T_B)$ of HPs evaporators, diethyl ether, which is the working fluid in the capillary-porous evaporators, starts to boil and produce large amount of vapour. The vapor pressure increases to values of $P^*$, at which the boiling point of diethyl ether is less than the evaporator temperature $T_{ev}$, and the process of evaporation stops.

The pressure pulsations with amplitude up to $3 \cdot 10^{-4}$ Pa spread through a vapour channel and condense in the cooled part of HPs. The vapor pressure decreases, the rarefaction wave comes to the evaporator and the next cycle of vapour formation and its moving to the HPs condensation zone begins.

The frequency of pulsations in the Laval-like vapour channel is larger than the pulsations in the HPs with the standard cylindrical vapour channel. The obtained values of the pulsations frequencies are given in table.

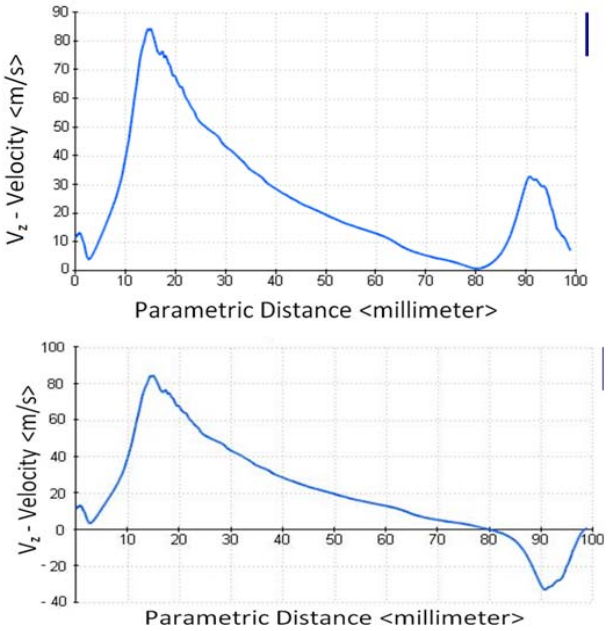


Fig. 5. The distribution of the axial component of velocity of the moist vapour inside the vapour channel of Laval-like HPs along the HPs centerline. Upper pattern with a positive velocity peak near the condensation surface of Laval-like HPs represents the velocity distribution along the longitudinal axis of vapour channel and inside the vortex ring. The figure on the bottom with a negative velocity value peak near the surface of condensation represents the velocity distribution along the longitudinal axis and outside of a vortex ring and shows the presence of a counter current due to the formation of a ring vortex near the HPs condensation surface. Overheating of the evaporator in reference to the boiling temperature of diethyl ether at atmospheric pressure is 15 K, the temperature difference between the evaporator and the condensation surface equals 25 K

Рис. 5. Распределение расчетных значений осевой составляющей скорости влажного пара внутри выполненного в виде сопла, близкого к соплу Лаваля, парового канала ТТ. Перегрев испарителя относительно температуры кипения диэтилового эфира 15 К, разница температур между испарителем и поверхностью конденсации ТТ в калориметре 25 К

**Pulsation rate values**

| Overheating of the evaporator, $\delta T$, K | Pulsation frequency $f_1$, Hz | Pulsation frequency $f_2$, Hz |
|---|---|---|
| 9.05 | 386 ± 5 | – |
| 10.1 | 396 ± 5 | – |
| 11.03 | 426 ± 5 | 406 ± 5 |
| 12.15 | 450 ± 5 | 420 ± 5 |
| 13.0 | 456 ± 5 | 437 ± 5 |
| 14.07 | 474 ± 5 | 440 ± 5 |
| 15.03 | 474 ± 5 | 454 ± 5 |
| 16.0 | 478 ± 5 | 453 ± 5 |
| 17.1 | 490 ± 5 | 460 ± 5 |
| 18.06 | 491 ± 5 | 472 ± 5 |
| 19.02 | 495 ± 5 | 473 ± 5 |
| 20.12 | 502 ± 5 | 474 ± 5 |

Table shows the pulsation rate values (modulation rate), obtained in the Laval-like HP, $f_1$ [Hz], and in the HP with standard cylindrical vapour channel, $f_2$ [Hz], depending on overheating $\delta T$, [K], of the evaporators.

Both HPs have equal outer diameters 20 mm and equal sectional areas of capillary-porous inserts near the condensation region. As the overheating of the evaporator $\delta T \sim 20$ K increases, pulsation frequency in the Laval-like nozzle goes up to ~ 502 Hz, the derivative of the relationship between pulsation frequency and temperature is approximately 10.5 Hz/K. While investigating HPs with standard cylindrical vapour channel and equal outer diameter of 20 mm, length of 100 mm and thickness of the evaporator and capillary-porous insert of 3 mm, initial pulsed flows occur in event of overheating of the evaporator $\delta T \sim 11$ K, frequency $f \sim 406$ Hz. As the overheating of the evaporator $\delta T \sim 20$ K increases, pulsation frequency in the cylindrical vapour channel goes up to 474 Hz, the derivative of the relationship between pulsation frequency and temperature is approximately 7.5 Hz/K.

The insensitivity zone of the capacity sensors in the cylindrical channel, defined by the initial convective nature of the vapour flow, is greater than in the vapour channel of Laval-like HPs. Measuring inaccuracy does not exceeds 3–5 Hz.

**Numerical model details.** Numerical simulations of the vortex pulsation flows inside a vapour channel of the Laval-like HP have been performed in finite element modeling in CFD 10.0 2D Fluent 6.3.26 under double precision axis-symmetric conditions. Navier–Stokes equations with measured boundary conditions were solved, using fixed temperature values of heat source and heat outlet. The model was studied as a longitudinal section along the axes of the two injector channels. It helps to preserve all the specific features of whirling instability under the conditions of continuous circulation motion of the working fluid during liquid and vapour phases. In the construction of the design model about 457233 finite elements were used, with increased meshing at injection capillary channels sections, nozzle throat section and turbulence element. The model size is a compromise between available computer resources and computational investigation error.

Transition from a stationary convective flow regime in the vapour channel to a pulsatile flow regime is clearly visible. At high heat capacity, received by the HPs, and boiling in the grid evaporator, excessive vapour occurs in the convergent part of the nozzle, leading to pressure increase up to the value, at which the average temperature of layers of the flat grid evaporator becomes lower than the boiling temperature of the working fluid, and boiling in the evaporator stops. Excessive vapour spreads through the divergent part of the vapour channel to the cooled area of the HP and is partially condensed. Due to the condensation effect, the pressure in the vapour channel decreases and the boiling process in the flat evaporator proceeds. Pressure increase period, vapour wave spreading in the condensation area of the HP and return expansion wave define the pulsation period in the vapour channel.

The results of flow simulation of compressible supersaturated vapour environment inside a vapour channel. The figure presents test values of the vapour flow pulsation in the vapour channel in the Laval-like form of the HPs. There are seven steps of calculation of the moist vapour flow velocity, from up to down. When boiling in the capillary-porous insert and the initial velocity of the flow of the two-phase vapour directly over the surface of the evaporator is 0.5–1 m/s in the throat section of the nozzle the axial flow velocity reaches 5 m/s and more. Obvious occurrence of pulsations, pulsation frequency rises, what is consistent with the experimental results [6; 7].

**Validation of numerical scheme.** Evident conversion from convection mode to convection-vortex mode and then to pulsation mode of the vapour flow inside of the HP is recorded at evaporator overheating value $\delta T \sim 9$ K.

Maximum value of velocity of diethyl ether moist vapour flow, obtained using calculation method in the throat section of the vapour channel using the colour indication of the software CFD Design 10.0, reaches 100–110 m/s when pulsation occurs, fig. 5. This fact gives the opportunity to evaluate the Reynolds number Re of the vapour channel during pulsation, which is defined by the formula:

$$\mathrm{Re} = \frac{\rho_{vp}^{\mathrm{mix}} u_{vp} D_C}{\eta_{\mathrm{mix}}}. \qquad (3)$$

We substitute moist vapour density (vapour and drops) [14; 15] $\rho_{vp}^{\mathrm{mix}} \sim 3$ kg/m$^3$, dynamic coefficient of viscosity of the moist vapour $\eta_{\mathrm{mix}} \sim 8 \cdot 10^{-6}$ Pa·s; maximum value of the vapour flow velocity (colour indication) near the throat section of the vapor channel $u_{vp} \sim$ (100–110) m/s; critical diameter of the vapour channel $D_C \sim 4 \cdot 10^{-3}$m, and obtain the value $\mathrm{Re} \sim (1.5–1.65) \cdot 10^5$, the Prandtl number $Pr = 0.77$.

Duration of the pulsation period $\Delta\tau_0$ inside the divergent part of the HPS vapour channel can be estimated using the formula:

$$\Delta\tau_0 \sim \frac{\Delta l}{u_{vp}}. \qquad (4)$$

Then substitute values of distance between pulsation crests (maximums) obtained in fig. 6 $\Delta l \sim (2–3) \cdot 10^{-2}$ m, moist vapour flow velocity in divergent part of the vapour channel obtained using colour indication by the software CFD Design 10.0 $u_{vp} \sim$ (20–30) m/s, and you will obtain numerical value of duration of the pulsation $\Delta\tau_0 \sim (0.75–1.5) \cdot 10^{-3}$ s.

**Analytical evaluation.** Evaporation cycle in the HPs exist at low heat load of the evaporator, up to 4–6 W/cm$^2$, and is characterized by convective flow in the vapour channel. Evaporation cycle of short HPs, when evaporator heating power is constant and maximum value is limited to prevent the development of bubble boiling in the flat grid evaporator, is defined in the following way:

$$E = \frac{\Delta Q}{\Delta\tau} < E_B, \qquad (5)$$

where $\Delta Q$ is heat energy, absorbed in the evaporator over a period of $\Delta\tau$, J; $\Delta\tau$ is time, sec; $E_B$ is thermal power, wherein the process of bubble boiling begins in the grid evaporator, W.

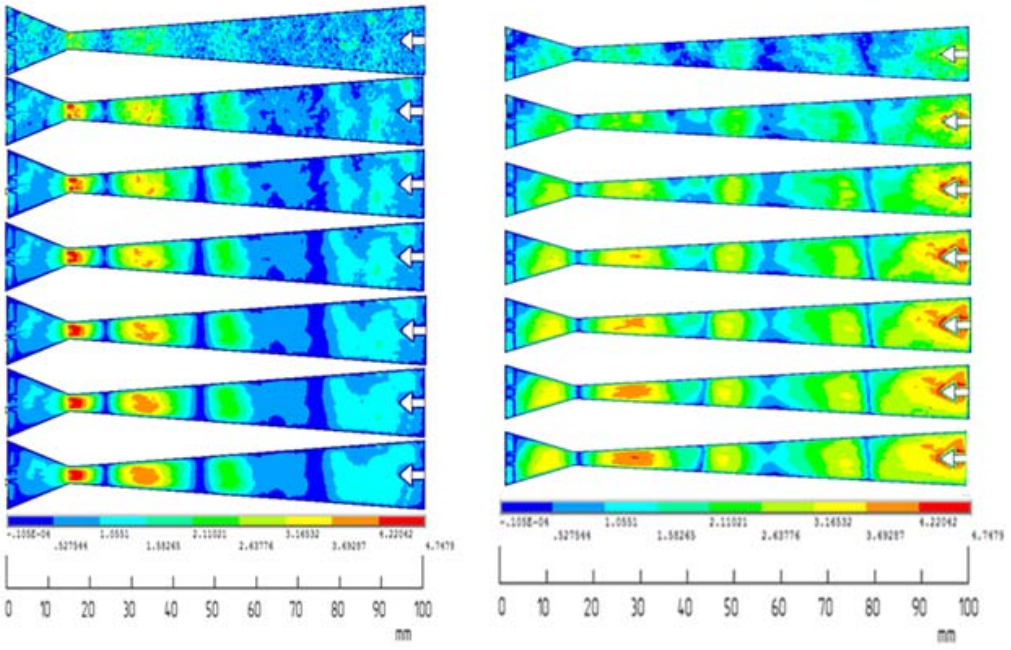


Fig. 6. The results of flow simulation of compressible supersaturated vapour environment inside a vapour channel. The figure presents test values of the vapour flow pulsation in the vapour channel in the Laval-like form of the HPs. There are seven steps of calculation of the moist vapour flow velocity, from up to down. When boiling in the capillary-porous insert and the initial velocity of the flow of the two-phase vapour directly over the surface of the evaporator is 0.5–1 m/s in the throat section of the nozzle the axial flow velocity reaches 5 m/s and more. Obvious occurrence of pulsations, pulsation frequency rises, what is consistent with the experimental results [6–7]

Rate of evaporation of dry monomolecular vapour over the evaporator is defined by the following equation:

$$\dot{M} = \dot{n}_{vp}\, m_{vp} = \frac{E}{r(T_B)}, \tag{6}$$

where $\dot{M}$ is the amount of the dry vapour, generated over the evaporator per time unit, kg/s; $\dot{n}_{vp}$ is the velocity of growth of the number of vapour molecules over the evaporator per time unit, $s^{-1}$; $m_{vp}$ is the mass of molecule of diethyl ether, kg; $r(T_B)$ is specific vaporization heat of the diethyl ether in HPs, depending upon temperature and pressure, J/kg; $T_B(P)$ is the boiling temperature of the diethyl ether, K.

Mass flow of saturated dry monomolecular vapour over the evaporator is defined by the following equation:

$$G_{vp} = \dot{M} = F(z) n_{vp}(T_{ev}) m_{vp}\, u_{vp} = \\ = F(z) \rho_{vp}(T_{ev}) u_{vp} = \frac{E}{r(T_B)}, \tag{7}$$

where $G_{vp}$ is a mass flow of dry saturated vapour over the evaporator, kg/s; $n_{vp}(T_{ev})$ is an average number of dry vapour molecules in the unit volume over the evaporator, $m^{-3}$; $u_{vp}$ is an average velocity of the vapour phase, m/s; $\rho_{vp}(T_{ev})$ is vapour density of diethyl ether over the evaporator, kg/m$^3$; $T_{ev}$ is the temperature of the evaporator, K.

Growth rate of the number of molecules of vapour over the evaporator in the convergent region of the nozzle of the vapour channel, which defines excess pressure over the evaporator and mass flow of vapour in HPs, is calculated from the equation:

$$\dot{n}_{vp} \cong \frac{E}{r(T_B) m_{vp}} = \frac{E N_A}{r(T_B) \mu_{vp}}, \tag{8}$$

where $N_A$ is the Avogadro constant, $mol^{-1}$; $\mu_{vp}$ is molar mass of diethyl ether vapour, kg/mol.

Assuming approximately equal velocities and without considering the jet type nature of the flow pattern, the linear velocity of the hydrodynamic flotation of the vapour flow over the evaporator surface is calculated from the equation:

$$u_{vp} \cong \frac{\dot{n}_{vp}}{F(z) n_{vp}(T_{ev})} = \frac{E}{F(z) r(T_B) m_{vp} n_{vp}(T_{ev})} = \\ = \frac{E N_A}{F(z) r(T_B) \mu_{vp} n_{vp}(T_{ev})}. \tag{9}$$

Insert expressions (9) and (8) in the equation (7) to obtain the formula for calculation of molecular flow of the dry vapour over the evaporator:

$$G_{vp} \cong \rho_{vp}(T_{ev}) \frac{E N_A}{r(T_B) \mu_{vp} n_{vp}(T_{ev})}. \tag{10}$$

Hydrodynamic flow of saturated dry vapour is defined by pressure difference value between the evaporator and condensation region in HP, according to the formula:

$$G_{vp} \cong A \frac{\rho_{vp}(T_{cond}) F(z)^2 \left(P(T_{ev}) - P(T_{cond})\right)}{\eta L} = \\ = A \frac{F(z)^2 \Delta P_{vp}}{\eta L}, \tag{11}$$

where $A$ is nondimensional constant about a unit; η is coefficient of dynamic viscosity of dry vapour, Pa·s; $L$ is the length of the vapour channel of the HPs, m; $P(T_{ev})$ is vapour pressure under the HPs evaporator, Pa; $P(T_{cond})$ is vapour pressure near the condensation surface of the HPs, Pa; $\Delta P_{vp}$ is vapour pressure difference over the evaporator and near the condensation surface in the vapour channel of the HPs, Pa; $T_{cond}$ is temperature of the condensation surface, K.

Equate mass and hydrodynamic flow of saturated dry vapour, and obtain the following equation:

$$G_{vp} \cong A \frac{\rho_{vp}(T_{cond})F(z)^2\left(P(T_{ev}) - P(T_{cond})\right)}{\eta L} =$$

$$= \rho_{vp}(T_{ev}) \frac{EN_A}{r(T_B)\mu_{vp}n_{vp}(T_{ev})}. \quad (12)$$

Excess pressure over the evaporator defines transfer of the vapour flow in the vapour channel of the HPs, and is calculated in linear approximation according to the equation:

$$P(T_{ev}) \cong P(T_{cond}) + \frac{dP}{dT}(T_{ev} - T_{cond}). \quad (13)$$

With respect to the Clapeyron–Clausius equation, the pressure derivative of the vapour by temperature is calculated in a conventional manner, nevertheless considering the fact that for liquid the specific volume ratio is small, $v^L / v^{vp} < 10^{-2}$–$10^{-3}$, hence in the Clapeyron–Clausius equation the value of the specific volume of fluid $v^L$ is ignored, and in ideal gas state the following equation is obtained:

$$\frac{dP}{dT} = \frac{1}{T}\frac{r(T)}{\left(v^{vp} - v^L\right)} \cong \frac{1}{T_{cond}}\frac{r(T_{cond})}{v^{vp}} \cong$$

$$\cong \frac{\rho_{vp}(T_{cond})r(T_{cond})}{T_{cond}}, \quad (14)$$

where $v^{vp}$ is the specific volume of the saturated vapour, m$^3$/kg; $v^L$ is the specific volume of the diethyl ether on the liquid-vapour coexistence line, m$^3$/kg.

Substitute expression (10) in (8), and obtain the equation to calculate vapour quantity in the HP:

$$\frac{F(z)^2 r(T_{cond})\rho_{vp}(T_{cond})}{\eta L}(T_{ev} - T_{cond}) \cong$$

$$\cong \frac{EN_A}{r(T_{cond})\mu_{vp}n_{vp}(T_{ev})}. \quad (15)$$

Vapour temperature over the evaporator's surface with low evaporation and without boiling is defined by the equation (16):

$$T_{ev} \cong T_{cond} \times$$

$$\times\left(1 + \frac{EN_A\eta L}{\rho_{vp}(T_{cond})F(z)^2 r(T_{ev})^2 \mu_{vp}n_{vp}(T_{ev})}\right) \le T_B. \quad (16)$$

Steady-state evaporation conditions in HPs mean that the temperature in the evaporator does not exceed boiling temperature of the working fluid. Heating capacity of the HPs, W, is defined according to the following equation:

$$E \cong \frac{\rho_{vp}(T_{cond})F(z)^2 r(T_{ev})^2 \mu_{vp}n_{vp}(T_{cond})}{N_A\eta L T_{cond}} \times$$

$$\times(T_{ev} - T_{cond}) = K_{HP}\Delta T, \quad (17)$$

where $n_{vp}(T_{cond})$ is an average number of dry vapour molecules in the unit volume near the condenser, m$^{-3}$.

Heat transfer coefficient $K_{HP}$ at cross-section of the vapour channel of the HP is defined according to the following expression:

$$K_{\text{HP}} \cong \frac{\rho_{vp}(T_{cond})F(z)^2 r(T)^2 \mu_{vp}n_{vp}(T_{cond})}{N_A\eta L T_{cond}}. \quad (18)$$

When the rate of heat supply into the thin evaporator is high, its average temperature is greater than the boiling temperature of the working fluid during bubble boiling or vaporization. The hydrodynamic vapour flow at the converging region of the nozzle has no time to carry out heating capacity generated through boiling in the evaporator.

Vapour density and pressure increase and boiling temperature of the working fluid goes up until it exceeds average temperature of the evaporator. Upon pressure increase the boiling in the evaporator stops (slows), and an overpressure wave spreads in the vapour channel to the condensation region of the HPs, where the vapour becomes supersaturated and condenses. The condensation process is not instant, and when the evaporator's activity is slowed (stopped), condensation lasts until the pressure decreases to the vapour saturation pressure at the condensation temperature, thereafter the condensation process stops.

The slow process of saturated vapour pressure decrease, due to condensation, feeds back through the vapour channel of the HP back to the evaporator, and the boiling process resumes there.

Pressure pulsations in the vapour channel of the HPs result from boiling and intensive vapour generation in the evaporator, non-instantaneous mass-transfer through the vapour channel to the condensation region of the HP, and the slow condensation process, which provides pressure decrease in the condensation region at first and then in the evaporator of the HPs.

Following all described processes the next pulsed evaporation cycle resumes. The heating capacity, entering to the flat grid evaporator of the short HP, when the evaporator's temperature exceeds the boiling temperature $T_B(P)$ of the working fluid, is defined according to the next equation:

$$E = \frac{\left[T_{ev} - T_B(P)\right]F(z)}{R_{ev}(T)}. \quad (19)$$

It is considered that moist vapour stream is formed of two subsystems: microdrops stream system $G_{dr}$ and dry vapour stream system, $G_{vp}$. Rate of vaporization of the moist droplet vapour flow is defined in the standard way:

$$\dot{M} = G_{\text{mix}} = G_{vp} + G_{dr}. \quad (20)$$

For the purpose of simplification of the analytical model construction, the real droplet vapour flow over the evaporator, having microdrops dimensioned by complicated double-humped distribution function, Lee, Reges, Almenas, [16], is reported in terms of a mono-dispersal system of spherical microdrops with arithmetic middling

radius $r_a$, which is frequently used while analyzing two-phase droplet vapour flows:

$$r_a = \frac{1}{n_{dr}} \sum_{i=0}^{\infty} r_{dri} n_{dri}, \quad (21)$$

where $n_{dr}$ is the total number of microdrops of all sizes per unit volume of the droplet vapour flow over the evaporator, $1/m^3$ ; $n_{dri}$ is the number of microdrops of the diethyl ether with radius $r_{dri}$ per unit volume of the droplet vapour medium, $1/m^3$.

Considering the accepted assumption over spherical shape of microdrops, the expression for absolute moisture $\gamma$ of the droplet vapour flow is defined in the standard way:

$$\gamma = \frac{M_{dr}}{M_{dr} + M_{vp}} = \left[ 1 + \frac{\rho_{vp}}{\rho_{dr}} \left( \frac{3}{4\pi} \frac{1}{r_a^3 n_{dr}} - 1 \right) \right]^{-1}, \quad (22)$$

where $M_{dr}$ is total mass of microdrops per unit volume of the droplet vapour flow over the evaporator, kg; $M_{vp}$ is vapour mass per unit volume of the dry vapour flow over the evaporator, kg; $n_{dr}$ is the total number of microdrops of all sizes per unit volume of the droplet vapour flow over the evaporator, $1/m^3$; $n_{dr}$ is the total number of microdrops of all sizes per unit volume of the droplet vapour flow over the evaporator, $1/m^3$; $\rho_{dr}$ is density of microdrops of the diethyl ether, $kg/m^3$.

The density of moisture vapour $\rho_{vp}^{\text{mix}}(T_{ev})$ without taking into account the relative motion phases is:

$$\rho_{vp}^{mix}(T_{ev}) = \frac{\rho_{dr}\rho_{vp}}{\gamma\rho_{vp} + (1-\gamma)\rho_{dr}}. \quad (23)$$

Synergies between consumable and absolute mass concentrations of microdrops $\gamma_G$ or consumable and absolute moisture levels are defined according to the following relation:

$$\gamma_G = \frac{\gamma\psi}{(1-\gamma)+\gamma\psi}; \quad \psi = \frac{u_{dr}}{u_{vp}}. \quad (24)$$

The value $\gamma_G$ represents the relation between the quantity of the condensed droplet phase and the total quantity of the two-phase droplet vapour, and, considering the expression (22), is as follows:

$$\gamma_G = \left[ 1 + \frac{\rho_{vp}}{\rho_{dr}\psi} \left( \frac{3}{4\pi} \frac{1}{r_a^3 n_{dr}} - 1 \right) \right]^{-1} = \frac{G_{dr}}{G_{\text{mix}}}. \quad (25)$$

Mass flow rate of microdrops on the evaporator's surface is considered to be proportional to vaporization velocity and mass flow rate of the vapour:

$$G_{dr} \cong B \left( \frac{E}{r(T_{ev})} \right)^a \left( \frac{G_{vp}}{F} \right)^b, \quad (26)$$

where $a$ and $b$ are numerical coefficients; $B$ is a coefficient with account for thermophysical properties of the diethyl ether and structural parameters of the evaporator (porosity, typical dimension of channels and pores).

To evaluate the vapour quantity transported from the evaporator to the condensation region of the HP, equation (31) is used, where the microdrops subsystem contribution to the generation of overpressure of the two-phase droplet mixture over the evaporator $P(T_{ev})$ in the vapour channel is neglected:

$$G_{\text{mix}} = G_{vp} + G_{dr} \cong \frac{\rho_{vp}^{\text{mix}} F(z) \Delta P_{vp}}{\eta_{\text{mix}} L}. \quad (27)$$

As a result of the boiling process in the evaporator, the pressure of the vapour over the evaporator increases up to $P^*$, whereby the boiling process in the surface layers and further in the whole of the thin evaporator (3 mm thick) is slowed (stopped) due to the fact that average temperature of the evaporator $T_{ev}$ becomes lower than the boiling temperature $T_B$ of the working fluid in the evaporator under the increased pressure and the confined space:

$$T_{ev} < T_B(P^*). \quad (28)$$

Furthermore, pulsing of the overpressured vapour begins to spread to the condensation region through the vapour channel. Cessation of boiling and retarding of vaporization in the evaporator of the HP lead to significant reduction (cessation) of the heat release and decrease in moist vapour transportation along the vapour channel of the HP to the condensation region of the HP. The time period $\Delta\tau_{ev}$ of pressure increase up to $P^*$ and cessation of boiling in the capillary-porous evaporator is estimated in linear approximation in ideal gas state and laminar heat transfer inside of the vapour channel of the HP, according to the formula:

$$\Delta\tau_{ev} \cong \frac{\left[ P^* - P(T_{cond}) \right] F(z) L}{k_B T_{ev} n_{vp}} \cong \cong \frac{\left[ P^* - P(T_{cond}) \right] F(z) L r(T_B) m_{vp}}{E k_B T_{ev}}. \quad (29)$$

Surplus energy (increased pressure) release time $\Delta\tau_{\text{HP}}$ in the evaporating region, by means of vapour flow transfer to the condensation region of the HP, is estimated according to the following formula:

$$\Delta\tau_{\text{HP}} \cong \frac{E\Delta\tau_{ev}}{r(T_B)\rho_{vp}^{\text{mix}}(T_{ev})u(T_{ev})F(z)}. \quad (30)$$

Surplus pressure release time $\Delta\tau_{\text{HP}}$ partially determines the time value of oscillations of the vapour flow in the vapour channel of the HP, during which the vapour pressure pulse, arisen over the evaporator, reaches the HP condensation surface, and condenses partially. The time period $\Delta\tau_{cond}$ of pressure decrease up to $P(T_{cond})$ is estimated according to the formula:

$$\Delta\tau_{cond} \cong \frac{E\Delta\tau_{ev}}{r(T_{cond})\rho_{vp}^{mix}(T_{cond})u(T_{cond})F(z)}. \quad (31)$$

As a result of the liquid phase formation, pressure near the cooling condensation surface reduces to:

$$P^* \cong P(T_{cond}). \quad (32)$$

This leads to the slowing of heat transfer through the vapour channel, the rarefaction wave propagation from the condensation zone to the evaporator and the start of the next cycle of pulsed increase of the pressure near the evaporator's surface. Thus, cycle pulse duration $\Delta\tau_0$ in the vapour channel of the HP is:

$$\Delta\tau_0 \cong \Delta\tau_{ev} + \Delta\tau_{\text{HP}} + \Delta\tau_{cond} + \Delta\tau_{sound}. \quad (33)$$

The analysis of the obtained measured data of heat transfer over the evaporator shows that the designed HPs

work in the boiling mode. This fact is confirmed by influence of operating parameters of the vaporization process (heat flow density q and pressure $P(T_{ev})$) on the heat transfer coefficient α. The influence of these parameters is related to the similar influence of heat flow density and pressure over the bubble boiling in the substantial volume. Performed numerical estimation of parts of pulsation duration $\Delta\tau_0$ from the expression (33) show the following.

Pressure increase duration $\Delta\tau_{ev}$ over the HPs evaporator leads to increased values $\Delta\tau_{ev} \sim 10^{-1}$–$10^{-2}$ c, which means incomplete adequateness of flat model of estimation of evaporability in the evaporator. It is necessary to consider nonequilibrium volumetric vaporization with regard to the structure and porosity of the evaporator, temperature and moisture gradient in the boiling two-phase working fluid.

Moving duration $\Delta\tau_{HP}$ of the vapour cluster along the convergent-divergent HPs vapour channel at vapour flow velocity in the channel equal ~ 100–300 m/s, reaches $\Delta\tau_{HP} \sim (4.8–1.6)\cdot10^{-3}$ s, which is acceptable only in the case when sonic velocity in dry vapour is ~300 m/s and correspondingly large temperature gradients in the vapour channel.

Maximum duration of condensation period of moist vapour is also excessive and reaches $\Delta\tau_{cond} \sim 10^{-1}$–$10^{-2}$ s.

Duration of expansion wave motion from condensation region to the HP evaporator at sonic speed in moist vapour about 100 m/s does not exceed $\Delta\tau_{sound} \sim 1\cdot10^{-3}$ s.

Comparison of experimental measured results of pulsation period duration in the convergent-divergent vapour channel of short low temperature HPs $\Delta\tau_0 = (2–2.5)\cdot10^{-3}$ s with the valued $\Delta\tau_0 \sim (0.75–1.5)\cdot10^{-3}$ s obtained using numerical method and the software CFD Design 10.0 shows that they have good fit values.

Comparison of experimental measured results of pulsation period duration in the convergent-divergent vapour channel of short low temperature HPs $\Delta\tau_0 = (2–2.5)\cdot10^{-3}$ with estimated values obtained using analytical method shows excessive values of analytical results. Suggested simple theoretical model of the flat surface evaporation gives excessive values of pulsation period duration and does not fully correspond to acutely nonequilibrium evaporation processes in the grid capillary porous evaporator with boiling working fluid.

**Conclusions.**

1. Heat transfer coefficient of the short linear HPs with the Laval-like vapour channel reaches the value of $(22 \pm 1)\cdot10^3$ W/m$^2$K; heat transfer coefficient of the HPs with the cylindrical vapour channel does not exceed $(15 \pm 1)\cdot10^3$ W/m$^2$K, if thickness of the capillary-porous insert layer is 3 mm, diameter is 20 mm and length is 100 mm. Comparison of heat transfer coefficients in short HPs shows sufficient advantages of HP with the Laval-like vapour channel in contrast with standard cylindrical channel.

2. The pulsatile flow regime in the vapour channel of short linear HPs occurs when the working fluid in the evaporator starts to boil. Vapour density and pressure increase and boiling temperature of the working fluid goes up until it exceeds average temperature of the evaporator. Upon pressure increase, the boiling in the evaporator stops (slows), and an overpressure wave spreads in the convergent-divergent vapour channel to the condensation zone of the HPs, where the vapour becomes supersaturated, and condenses. Condensation of moist vapour results in pressure decrease in condensation region, and after arrival of the expansion wave at the HPs evaporator, pressure over the evaporator also decreases, the boiling process in the evaporator proceeds and the pulsation cycle in the vapour channel repeats.

3. Flow stagnation leads to vortex formation, and their interaction causes pulse-coupled vortex decay, static pressure boost and complex reverse flows. Calculation results show that flow stagnation during the pulsation cycle leads to an enlargement of the recirculating region and augmentation of condensation, and this effect is significant.

With all the operating parameters of heat pipes, two effects were observed: pulsating flow regime of two-phase vapour flow and film-type condensation.

## References


1. Akachi H. Structure of Heat Pipe. US patent 1990. № 4921041.

2. Tong B. Y., Wong T. N., Ooi K. T. Closed-loop pulsating heat pipe. *Applied Thermal Engineering*. 2001, Vol. 21, No. 18, P. 1845–1862.

3. Naik R., Varadarajan V., Pundarika G., Narasimha K. R. Experimental Investigation and Performance Evaluation of a Closed Loop Pulsating Heat Pipe. *Journal of Applied Fluid Mechanics*. 2013, Vol. 6, No. 2, P. 267–275.

4. Seryakov A. V. Velocity measurements in the vapour channel of low temperature range heat pipes. *International Journal of Engineering Research & Technology*. 2013, Vol. 2, No. 8, P. 1595–1603.

5. Gupta A. K., Lilley, D., Sayred N. Swirling flow. New York : Wiley. 1987. 588 p.

6. Seryakov A. V. Pulsation flow in the vapour channel of low temperature range heat pipes. *Direct Research Journal of Engineering and Information Technology*. 2014, Vol. 2(1), P. 1–10.

7. Seryakov A. V. Pulsation flow in the vapour channel of short low temperature range heat pipes. I*nternational Journal on Heat and Mass Transfer Theory and Application*. 2014, Vol. 2, No. 2, P. 40–49.

8. Seryakov A. V., Ananiev V. I., Orlov A. V. Condensation research in the short low-temperature range heat pipes. *Proceedings of the 9th Minsk International Seminar of Heat Pipes*, Heat Pumps, Refrigerators, Power Sources. Minsk, Belarus, 7–10 September 2015, Vol. 2, P. 168–176.

9. Seryakov A. V., Ananiev V. I. Condensation research in the short low-temperature range heat pipes. *Proceedings of the VIII International Symposium on Turbulence,* Heat and Mass Transfer. Sarajevo, Bosnia and Herzegovina, September 15–18 2015. Begell House Inc. P. 693–696.

10. Patent № 2431101 RF, F 28D 15/00/ Method of filling heat pipes. Seryakov A.V. Published 10. 10. 2011. Bulletin No. 28.

11. Utility model patent No. 152108. Capacitance sensor for determination of a fluid layer thickness. Seryakov A. V. Published on 27.06.2015. Bulletin No. 18/2015.

12. Seryakov A. V., Konkin A. V., Belousov V. K. Application of a jet steam nozzle in medium-temperature range heat pipes. *Bulletin of Siberian State Aerospace University*. 2012, iss. 1(41), P. 142–147.

13. Faghri A. Heat Pipe Science and Technology. 1995. Washington USA, Taylor and Francis. 367 p.

14. Vargaftic N. B. *Spravochnick po teplophizicheskim svoistvam gasov i zhidkostey* [Handbook of thermophysical properties of gases and liquids]. Moscow, Publishing house of Physico - Mathematical literature, 1963, 708 p.

15. Tables of physical values. Guide under the editorship of Kikoin I.K., the member of Academy of Science. Moscow : Atomizdat 1976. 1008 p.

16. Lee R., Reges J., Almenas K. Size and number density change of droplet populations above front during reflood. *International Journal of Heat and Mass Transfer*. 1984, Vol. 27, No. 4, P. 573–585.

**Библиографические ссылки**

1. Pat. 4921041 US. Structure of Heat Pipe / Akachi H. 1990.

2. Tong B. Y., Wong T. N., Ooi K. T. Closed-loop pulsating heat pipe // Applied Thermal Engineering. 2001. Vol. 21, № 18. P. 1845–1862.

3. Experimental Investigation and Performance Evaluation of a Closed Loop Pulsating Heat Pipe / R. Naik [et al.] // Journal of Applied Fluid Mechanics. 2013. Vol. 6, № 2. P. 267–275.

4. Gupta A. K., Lilley D., Sayred N. Swirling flow. New York : Wiley, 1987. 588 p.

5. Seryakov A. V. Pulsation flow in the vapour channel of low temperature range heat pipes // Direct Research Journal of Engineering and Information Technology. 2014. Vol. 2(1). P. 1–10.

6. Seryakov A. V. Pulsation flow in the vapour channel of short low temperature range heat pipes // International Journal on Heat and Mass Transfer Theory and Application. 2014. Vol. 2, № 2. Pp. 40–49.

7. Seryakov A. V., Ananiev V. I., Orlov A. V. Condensation research in the short low-temperature range heat pipes // Proceedings of the 9th Minsk International Seminar of Heat Pipes, Heat Pumps, Refrigerators, Power Sources. (7–10 September 2015, Minsk). Vol. 2. P. 168–176.

8. Seryakov A. V., Ananiev V. I. Condensation research in the short low-temperature range heat pipes // Proceedings of the VIII Intern. Symposium on Turbulence, Heat and Mass Transfer. (15–18 September 2015, Sarajevo, Bosnia and Herzegovina). Begell House Inc. P. 693–696.

9. Пат. 2431101 RF, F 28 D 15/00. Способ заполнения тепловых труб / Серяков А. В. Опубл. 10.10.2011, Бюл. 28.

10. Полезная модель 152108. Емкостный датчик для определения толщины слоя жидкости / Серяков А. В. Опубл. 27.06.2015, Бюл. № 18/2015.

11. Серяков А. В., Конькин А. В., Белоусов В. К. Применение струйного парового сопла в тепловых трубах среднетемпературного диапазона // Вестник СибГУ. 2012. Вып. 1(41). С. 142–147.

12. Seryakov A. V. Velocity measurements in the vapour channel of low temperature range heat pipes // International Journal of Engineering Research & Technology. 2013. Vol. 2, № 8. P. 1595–1603.

13. Faghri A. Heat Pipe Science and Technology. Washington : Taylor and Francis, 1995.

14. Варгафтик Н. Б. Справочник по теплофизическим свойствам газов и жидкостей. М. : Физматгиз. 1963. 708 с.

15. Таблицы физических величин : справочник / под ред. акад. И. К. Кикоина. Атомиздат, 1976. 1008 с.

16. Lee R., Reges J., Almenas K. Size and number density change of droplet populations above front during reflood // International Journal of Heat and Mass Transfer. 1984. Vol. 27, № 4. P. 573–585.